Signal Integrity Analysis of the Structure with Single Modal Reservation Before and After Failures

Yevgeniy S. Zhechev, Artem V. Medvedev, and Talgat R. Gazizov

Abstract—To improve the reliability of radio electronic devices, engineers use redundancy of the most relevant circuits. The simplest and most common solution is classical cold redundancy in which the primary and redundant circuits are located far from each other. Meanwhile, locating the primary and redundant circuits close together makes it possible to use modal distortions to protect both circuits from unwanted ultra-wideband interference. This approach is known as modal redundancy or modal reservation (MR). This paper presents the results of signal integrity analysis for a structure with single MR before and after failures. It is shown that the bandwidth after failures changes. This affects the rate of data that can be excited to the input of the device without significant distortion of the useful signal. The authors used pseudo-random binary sequences with a data rate of 50 and 200 Mbps. It is experimentally shown that failures in the redundant circuit do not significantly degrade the quality of signal integrity in the bandwidth. Thus, the data-dependent jitter changes from 12 (before failures) to 19 ps (after the worst failure). In all investigated variants, the eye stays open; as a result, the bit error rate will be low. The mismatch of the redundant circuit has the largest effect on the noise amplitude. As a result, the signal-to-noise ratio decreases from 57 (before failures) to 28 (after the worst failure). To confirm the measurements, we performed electrodynamic simulations. Their results are in good agreement with the experimental data.

Index Terms—Signal integrity, eye diagram, electromagnetic compatibility, functional safety, data-dependent jitter, modal reservation, printed circuit board, failure.

I. Introduction

WHEN developing new methods to ensure functional safety and electromagnetic compatibility (EMC), engineers must consider three effects that cause disruption of electronic devices when ultra-wideband (UWB) interference occurs in the interconnection. These effects include: irreversible failures of some elements, transition of active elements into the saturation mode, and errors in the transmission of digital signals [1].

Traditionally, engineers use cold redundancy to improve reliability and functional safety. However, this solution does not protect radio electronic devices (REDs) from UWB interference. Modal reservation (MR) is a new approach to the assembly and tracing of printed circuit board (PCB) interconnections, characterized by strong electromagnetic coupling between the reserved (primary) and reserving (redundant) circuits of REDs. Fig. 1 shows the main differences between classical cold redundancy and MR. It can be seen that in the case of classical redundancy, two identical circuits are implemented on two different PCBs pressed against a metal plate. In the case of MR, two identical circuits are implemented on the same PCB, with strong electromagnetic coupling between the reserved and reserving circuits. This allows employing modal distortions to protect circuits from UWB interference.

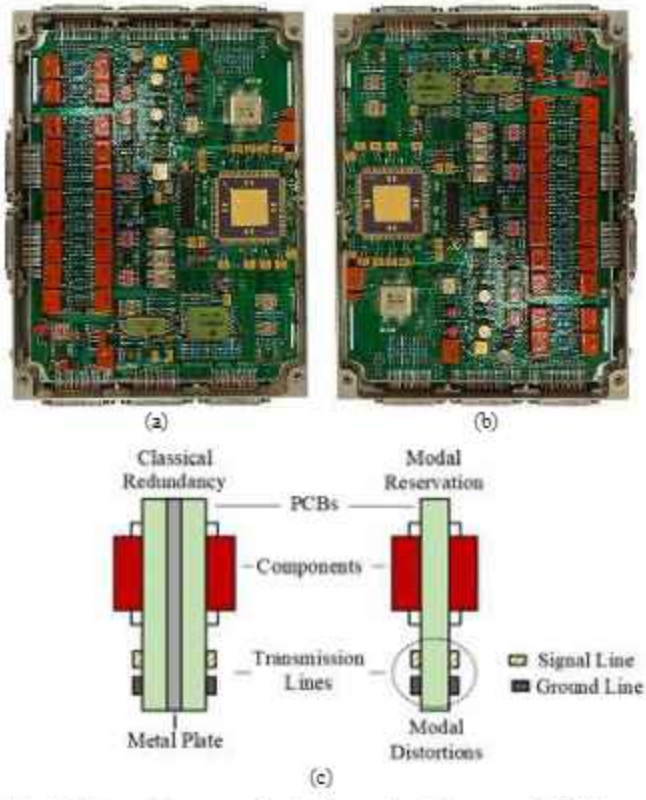

Fig. 1. Photos of the reserved (a) and reserving (b) spacecraft PCBs on the metal plate with classical cold redundancy and the illustration of differences between classical redundancy and MR (c).

In the previous study [2], we presented the results of an experimental study of the structure with single MR before and after failures. In that case, the frequency and time characteristics were analyzed only from the perspective of UWB interference suppression. Fig. 2 shows modal decomposition of the UWB pulse in the structure with MR. We can see that such structure may protect electrical circuits from UWB interferences by decreasing the out-

The measurement was funded by the Russian Science Foundation, project 19-19-00424 (https://rscf.ru/project/19-19-00424/) at TUSUR. The modeling and simulation were supported by the Ministry of Science and Higher Education of the Russian Federation, project FEWM-2022-0001. (Corresponding author: Yevgeniy S. Zhechev). The authors are with the Tomsk State University of Control Systems and Radioelectronics, Tomsk 634050, Russia (e-mail: zhechev75@gmail.com; medart20@rambler.ru; talgat@tu.tusur.ru).

put voltage amplitude (e.g. from 264 V to 39 V). Structures with classical cold redundancy has no effect on the amplitude of the UWB interference.

Structures with MR may be used in transmission systems that require high quality of the useful signal. After failure of the reserved circuit, the reserving circuit takes over its functions (Fig. 3). More specifically, a switching device (SD) based, for example, on T-type switches [3] switches the signal source to the reserving conductor. Failures of a component with load R can either be in the form of an open circuit (OC) or a short-circuit (SC) to ground. For example, before failures, Conductor 1 (C1) is working, and Conductor 2 (C2) is the reserving (Fig. 3a). After a failure at the end of C1, the SD switches the source to C2, and either a SC or OC occurs at one end of C1 (Fig. 3b). Changing the terminations in the neighboring circuit can affect signal integrity. Thus, the aim of this work is to perform a signal integrity analysis of the structure with single MR before and after failures.

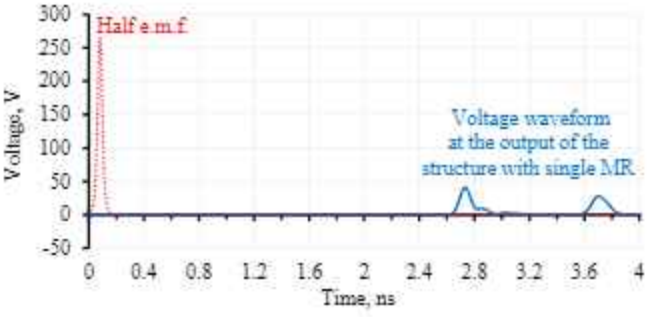

Fig. 2. Voltage waveforms at the input and output of the structure with MR obtained for the UWB pulse with total duration of 150 ps.

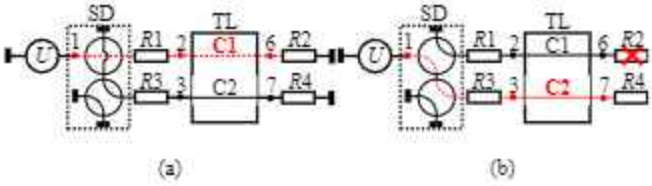

Fig. 3. Switching diagrams of the structure with single MR before (a) and after (b) failure.

II. Analysis Techniques

The initial characteristics and geometrical parameters of the structure with singe MR under investigation were presented in [2]. As in the case of the UWB interference analysis, we used connection diagrams for the structure, simulating cases before and after failures (Fig. 4). The cross-section of the regular part of the structure with MR is shown in Fig. 4d. All resistors shown in the diagram are 50 Ω. In this study, a pseudo-random binary sequence (PRBS) source of 50,000 bits and data rates of 50 and 200 Mbps (separately) were used. These data rates were conditioned by the bandwidth of the structure with MR after failure. The rise time (t_r) and the fall time (t_f) were 4 and 1 ns; the duration of the unit interval (T) was 20 and 5 ns, and the e.m.f. was 5 V. At the first stage, we obtained the frequency characteristics of the structure before and after failures using a vector network analyzer (VNA) (Panorama P4226) in the frequency range from 10 to 200 MHz. Next, the Advanced Design System (ADS) was used to obtain time domain responses. To analyze signal integrity, the response to a single PRBS pulse was obtained for the cases before and after failures. Fig. 4 shows diagrams of frequency response measurements and time response analysis in the ADS.

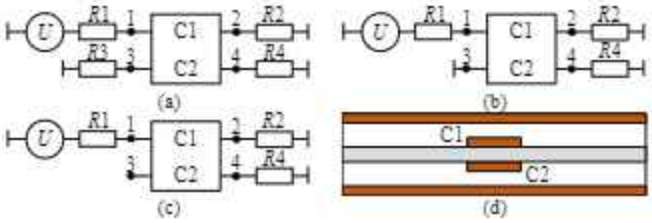

Fig. 4. Equivalent connection diagrams for simulating the failures of the reserved conductor: without failures (a), SC at the input (b), OC at the input (c), and the cross-section of the structure (d).

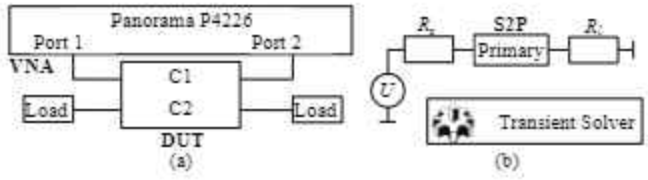

Fig. 5. Diagrams of frequency response measurements (a) and time response analysis in the ADS (b).

To confirm the measurement results, we performed electrodynamic simulation of the frequency and time characteristics of the structure with MR in the ADS. We used the method of moments and conducted simulations in the frequency range from 0 to 200 MHz. In this case, the grid density was 20 cells per wavelength. The conductors were additionally divided into separate cells to take into account the edge effects.

III. Frequency and Time Domain Results

Figs. 6 and 7 show the frequency dependences of $|S_{11}|$ and $|S_{21}|$ obtained in the measurements and simulations for the structure before and after failures.

For the case before failures (50-50), short-circuit at the input (SC-50), and open-circuit at the input (OC-50), the bandwidths are 70, 57, and 199.5 MHz, respectively. The differences between the SC-50 and OC-50 cases and the 50-50 case by 0.8 and 2.8 times, respectively, can be explained by different boundary conditions at the near end of the structure. We can see that the measurement results agree with the simulation ones. The selection of the data rate should be conditioned by the bandwidth of the structure with MR before and after failures. For the structure under investigation the lowest cutoff frequency was 57 MHz. However, the highest cutoff frequency after failure was 199.5 MHz. Therefore, next we analyzed two PRBSs with the rates of 50 and 200 Mbps. The $|S_{11}|$ values for the 50-50, SC-50, and OC-50 cases do not exceed -20, -6.5, and -7.6 dB in the bandwidths, respectively. It can be seen that for the cases after failures the reflections at the near end of the reserved conductor will be greater than for the case before failures.

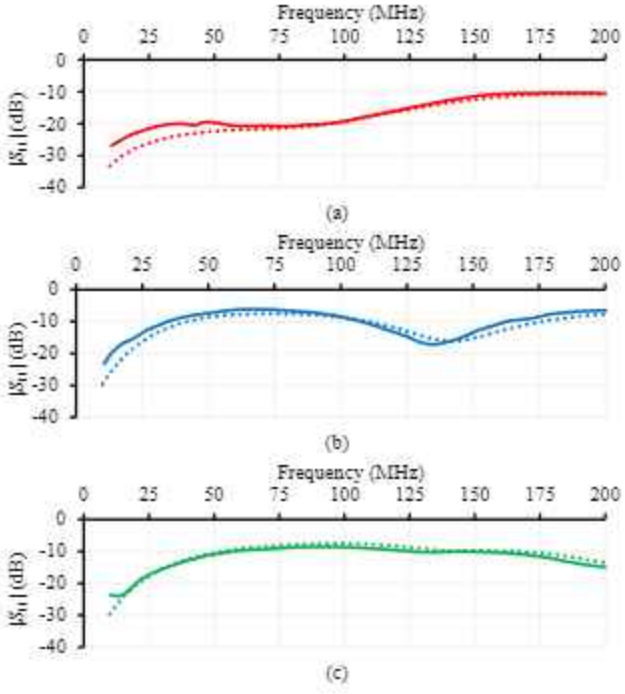

Fig. 6. Frequency dependences of $|S_{11}|$ up to 200 MHz obtained during measurements (–) and simulations (···) under boundary conditions at the ends of the reserved conductor at 50-50 (a), SC-50 (b), and OC-50 (c).

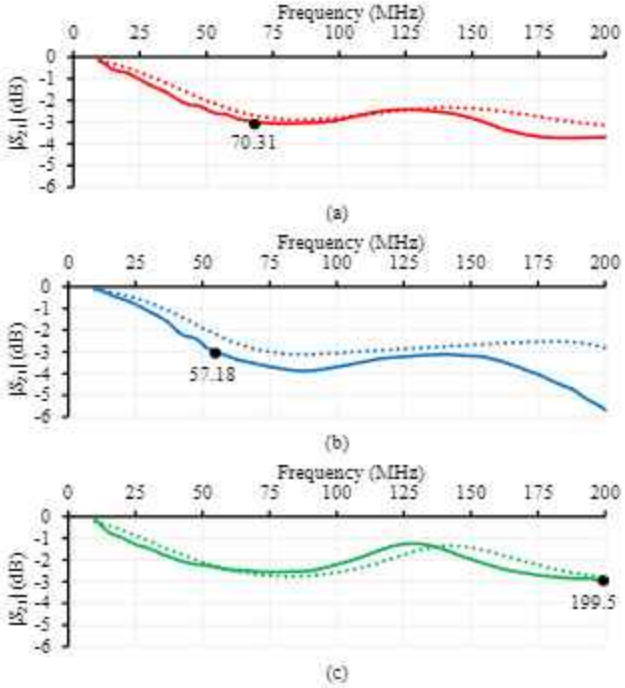

Fig. 7. Frequency dependences of $|S_{21}|$ up to 200 MHz obtained during measurements (–) and simulations (···) under boundary conditions at the ends of the reserved conductor at 50-50 (a), SC-50 (b), and OC-50 (c).

Fig. 8 shows the phase-frequency characteristics of $|S_{21}|$ for the structure before and after failures. They show that the characteristics for all the considered failures have a common form. However, the highest slope was observed for the case of SC-50, and the lowest – for OC-50. At the same time, we can see that for all variants, the phase distortion of the signal is

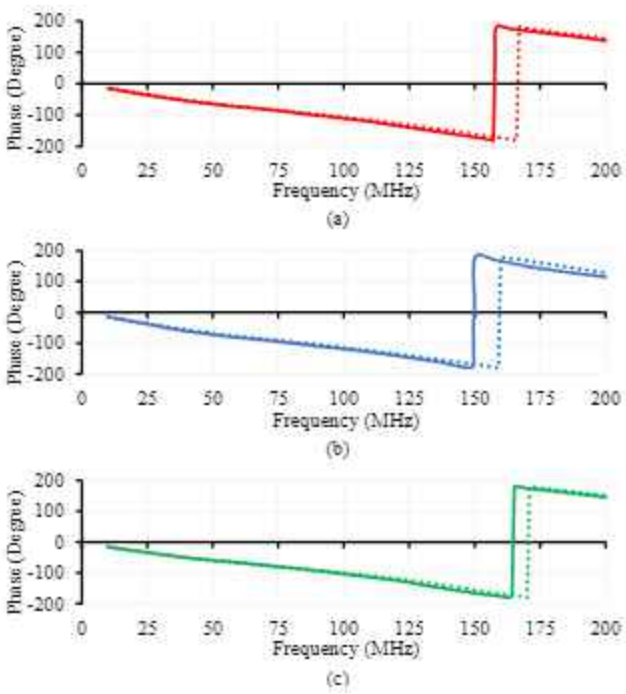

Fig. 8. Phase of the received signal at Node 2 obtained during measurements (–) and simulations (···) under boundary conditions at the ends of the reserved conductor at 50-50 (a), SC-50 (b), and OC-50 (c).

minimal. The measurement results also agree well with the simulation results.

Fig. 9 shows the time responses to a single PRBS pulse at Node 2 before and after failures. We can see that the voltage waveforms have similar behavior. Meanwhile, the types of failure affect t_r and t_f differently. For the pulse with the rise time of 4 ns the maximum amplitude of all pulses does not exceed 2.15 V, which indicates the presence of losses in the structure. In the case of a signal with a rise time of 1 ns, strong distortions are observed. The maximum amplitude in this case does not exceed 2.1 V.

Fig. 10 shows the eye diagrams obtained when the PRBS was propagating through the structure with MR before and after failures. Table I summarizes the main parameters of the useful signal obtained during the measurements. In the figure, we can see a temperature view of the 3-dimensional eye diagrams. The eye is automatically centered and displayed over 2T on the horizontal axis. The color indicates the number of crossings of a segment in the time-voltage plane. Blue areas are cold, whereas red indicates comparatively more crossings. During simulation, we computed contours of constant error probability and added them to the eye diagrams as BERContour. This method allows a comparative analysis of simulation and experiment results.

We can see that signal integrity is ensured even in the case of failure. Thus, for the 50 Mbps bitrate, the data-dependent jitter changes from 47.5 ps (50-50) to 19 ps (OC-50). For the 200 Mbps bitrate, it changes from 63 ps (OC-50) to 68.8 ps (SC-50). In all investigated cases the eye is still open, therefore the likelihood of bit errors will be low. The mismatch of the reserved circuit has the greatest effect on the amplitude noise. As a result, for the 50 Mbps

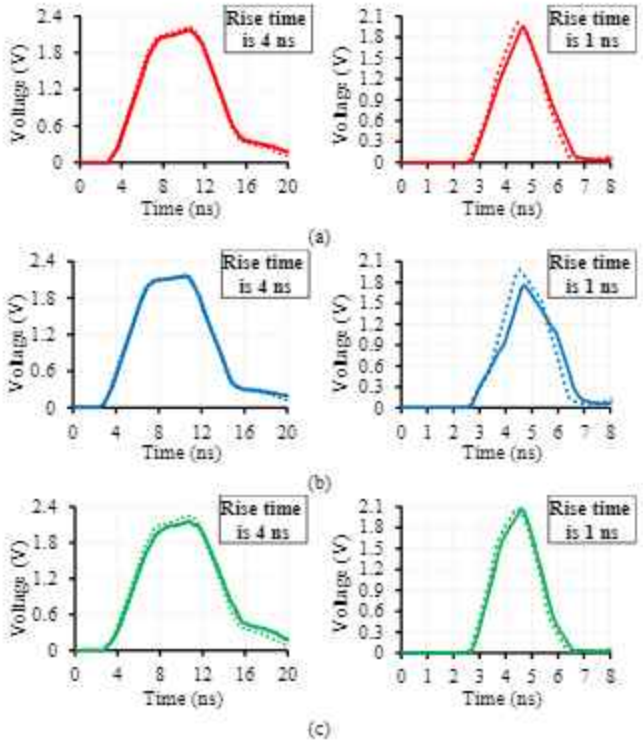

Fig. 9. Voltage waveforms of pulses the with rise time of 4 ns (left) and 1 ns (right) at the far end of the structure obtained during measurements (–) and simulations (···) under boundary conditions at the ends of the reserved conductor at 50-50 (a), SC-50 (b), and OC-50 (c).

bitrate, the signal-to-noise ratio decreases from 57 (50-50) to 28 (OC-50). For the 200 Mbps bitrate, the minimal value of this parameter is 4.89 (SC-50). The analysis of the 200 Mbps rate showed that, after OC-50 failure, the eye is better than before the failure. This may be due to a greater bandwidth of the structure after failure. The eye diagrams show that the investigated structure with MR may be used to transmit a useful signal even at 200 Mbps.

TABLE I
Useful Signal Parameters

Parameters	50-50		SC-50		OC-50	
	50 Mbps	200 Mbps	50 Mbps	200 Mbps	50 Mbps	200 Mbps
Jitter, ps	12	63	15	69.8	19	47.5
Eye width, ns	9.99	2.38	9.98	2.47	9.97	2.48
Eye height, V	2.3	1.57	2.17	1.45	2.11	1.66
Amplitude noise, mV	65	410	90	520	130	410
Signal-to-noise ratio	57	7.55	39	4.89	28	9.11

IV. Potential Application Area

Based on the obtained results, including those from previous works [4]–[6], the potential area of MR application can be determined. In [4], a preliminary quasi-static simulation of an MR-based PCB prototype with a length of 0.324 m was performed before and after failures in the time and frequency domains. In [5], quasi-static and electrodynamic simulations of the MR-based PCB mock-ups with the lengths of 0.141, 0.185,

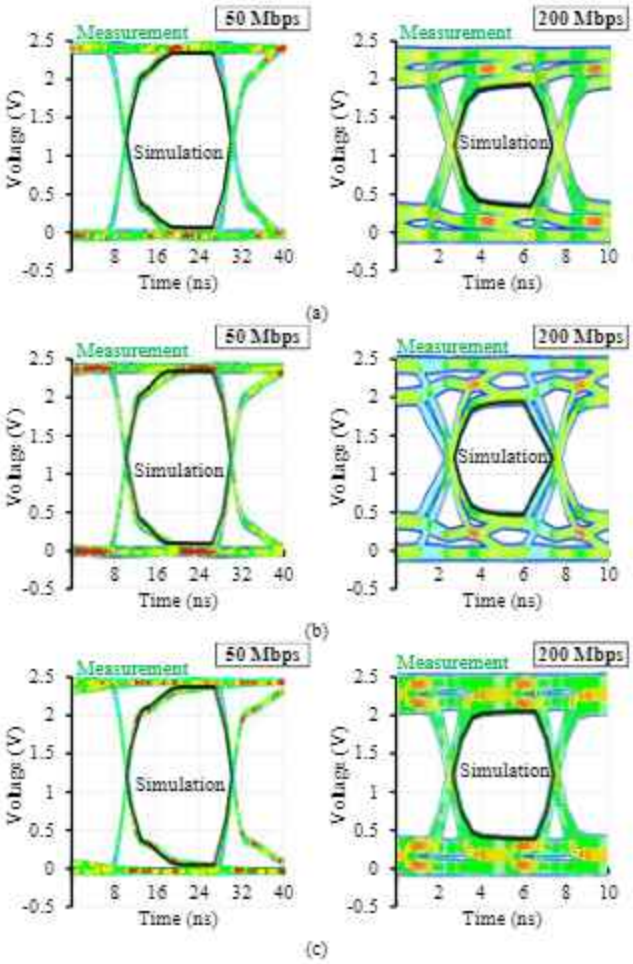

Fig. 10. Eye diagrams for the structure with single MR obtained during measurements (–) and simulations (···) for configurations 50-50 (a), SC-50 (b), and OC-50 (c).

and 0.324 m were performed before and after failures in the frequency domain. In [2], a 0.324-m-long PCB layout was studied experimentally before and after failures, and N-norms were calculated showing the probability of various component failures. In this paper, the integrity of the signal of this layout has been investigated.

Many digital systems operate close to 100 MHz [6]. An example is CDC421A106 [7] (Texas Instruments), which is a high-performance clock generator with low phase noise. Its total jitter is 35 ps at a clock frequency of 100 MHz. This study considered the MR-based structure that can be used in systems up to 200 MHz. However, if the length of the structure is reduced, then the bandwidth will increase, which was demonstrated in [5]. Therefore, it is necessary to control the bandwidth and the stopband for the interconnections of the end device, thus increasing noise immunity of REDs. The maximum length of conductors is usually limited by the PCB dimensions. There are several form factor standards [8] that are used for high performance systems for space applications, for example, CompactPCI, SpaceVPX, MicroTCA and PC/104. They show that the optimal length of PCB interconnections is up to 0.2 – 0.3 m.

V. Conclusion

This paper discusses signal integrity in the structure with singe MR first presented in [2]. It is shown that the bandwidths for the SC-50 and OC-50 failure cases differ from the 50-50 variant. This affects the bitrate that can be excited to the input of the device without significant distortion of the useful signal. It was revealed that preceding transmitted bit sequences can affect the front and amplitude of succeeding pulses. Thus, for the 50 Mbps bitrate, the signal-to-noise ratio decreases from 57 (50-50) to 28 (OC-50). This decrease is caused by the interference of incident and reflected waves, crosstalk, dispersion, and different velocities of mode propagation along the structure. This leads to the appearance of density distribution of the probability of deviation of the phase and amplitude jitter. Nevertheless, the results show that the signal quality degrades insignificantly in the case of failure. The jitter values are typical for stripline and microstrip devices. Thus, for the 50 Mbps bitrate, the data-dependent jitter changes from 12 ps (50-50) to 19 ps (OC-50). For the 200 Mbps bitrate, it changes from 63 ps (OC-50) to 68.8 ps (SC-50). Unexpected was the result obtained in the case of the OC-50 which showed that the bandwidth was significantly expanded. This expansion might have been caused by the fact that, because of multiple re-reflections, standing waves occur in the structure and affect the frequency characteristics. Comparison of the experimental and electrodynamic simulation results showed their good convergence.

Thus, the results obtained supplement the previously published work on the experimental study of the structure with single MR before and after failure. The conclusions will be useful in the design of real transmission lines with MR.

References

1. L.N. Zdoukhov, Yu.V. Parfenov, O.A. Tarasov, V.M. Chepelev, "Three possible mechanisms for the failure of electronic devices as a result of electromagnetic interference," in Technologies of electromagnetic compatibility, vol. 2, no. 65, pp. 22-34, 2018.
2. A.V. Medvedev, Y.S. Zhechev and T.R. Gazizov, "Experimental study of a structure with single modal reservation before and after failure," in IEEE Trans. Electromag. Compat., vol. 64, no. 4, pp. 1171-1181, 2022, doi: 10.1109/TEMC.2022.3171770.
3. K.Y. Chan, M. Daneshmand, A. A. Fomani, R. R. Mansour, and R. Ramer, "Monolithic MEMS T-type switch for redundancy switch matrix applications," 2008 38th European Microwave Conference, Oct. 2008.
4. A. V. Medvedev, T. R. Gazizov, and Y. S. Zhechev, "Evaluating modal reservation efficiency before and after failure," Journal of Physics: Conference Series, vol. 1488, no. 1, p. 012015, Mar. 2020.
5. A. V. Medvedev and Y. S. Zhechev, "Analysis of frequency characteristics of a structure with single modal reservation before and after failure," IOP Conference Series: Materials Science and Engineering, vol. 862, p. 022037, May 2020.
6. C.F. Coombs, Printed Circuits Handbook, The McGraw-Hill Companies, 2008.
7. M. Kubicek, "In-system jitter measurement using FPGA," in 20th International Conference Radioelektronika 2010, Brno, Apr. 2010, pp. 1– 4.
8. J.R. Marshall and R.W. Berger, "Maturation of a scalable form factor system standard for interoperable spaceborne processing and interconnect needs: Missions and applications, short paper," 2016 International SpaceWire Conference (SpaceWire), Oct. 2016.

Author Biographies

Yevgeniy S. Zhechev *was born in Almaty, Kazakhstan, in 1994. He received the B.Sc. and M.Sc. degrees in Infocommunication Technologies and Communication Systems from Tomsk State University of Control Systems and Radioelectronics, Tomsk, Russia, in 2016 and 2018, respectively. Currently, he is a Ph.D. student in Electromagnetic Compatibility of Radioelectronic Devices. He has over five years of experience with electromagnetic compatibility issues. His current research interests include time-domain electromagnetic modeling techniques, electromagnetic compatibility, microwave transmission lines, and power protective devices. He has authored or coauthored over 60 refereed publications.*

Artem V. Medvedev *was born in Tomsk, Russia, in 1994. He received the B.Sc. and M.Sc. degrees in radio engineering and electromagnetic compatibility from the Tomsk State University of Control Systems and Radioelectronics, Tomsk, Russia, in 2017 and 2019, respectively. Currently, he is a Ph.D. student in electromagnetic compatibility of Radioelectronic Devices. He has over four years of experience with electromagnetic compatibility issues. His current research interests include electromagnetic compatibility, redundancy, and functional safety. He has authored or coauthored over 26 refereed publications.*

Talgat R. Gazizov *was born in Jalal-Abad, Kyrgyzstan, in 1963. He received the Ph.D. degree in Improvement of Circuit Board Interconnections and the D.Sc. degree in Reduction of Electric Signal Distortions in the Interconnections and Effects of Power Electromagnetic Interference from Tomsk State University of Control Systems and Radioelectronics, Tomsk, Russia, in 1999, and 2010, respectively. He has authored/coauthored more than 430 scientific papers, including 11 books. His research interests include signal integrity problems.* **EMC**

IMS

2023 IEEE MTT-S INTERNATIONAL MICROWAVE SYMPOSIUM

11–16 JUNE
SAN DIEGO CONVENTION CENTER
SAN DIEGO, CALIFORNIA

Join Us in San Diego and Experience the Coolest Ideas Under the Sun!

IMS2023 is the centerpiece of Microwave Week 2023, which includes the RFIC Symposium (www.rfic-ieee.org) and the ARFTG Microwave Measurement Conference (www.arftg.org). It is the world's largest technical symposium and industry exhibition for MHz through THz professionals. IMS2023 will feature an exciting Technical Program that compliments this year's theme of Coolest Ideas Under the Sun – think high efficiency, thermal management, model-based design, space and aerospace systems, and so much more!

The Coolest Ideas Under the Sun

SAN DIEGO 2023

IMS2023 Conference Themes

At IMS2023, we will have several focus themes to highlight a number of areas of RF and microwave engineering that are of topical interest or impact. These themes are:

- Systems & Applications
- Space
- Biomedical Applications
- RF & Microwaves in Latin America

Interested in participating in IMS2023 as an attendee or exhibitor?
Scan the QR code to sign up for updates.

IEEE

MTT-S
IEEE MICROWAVE THEORY & TECHNOLOGY SOCIETY

For more information: ims-ieee.org/ims2023